Journal of Molecular Structure 934 (2009) 117–122

Contents lists available at ScienceDirect

Journal of Molecular Structure

journal homepage: www.elsevier.com/locate/molstruc

Modeling of a Tröger's tweezer and its complexation properties

Václav Parchaňský [a], Pavel Matějka [a], Bohumil Dolenský [a], Martin Havlík [a], Petr Bouř [b,*]

[a] Department of Analytical Chemistry, Institute of Chemical Technology, 166 28 Prague, Czech Republic
[b] Institute of Organic Chemistry and Biochemistry, Academy of Sciences, 166 10 Prague, Czech Republic

ARTICLE INFO

Article history:
Received 24 April 2009
Received in revised form 22 June 2009
Accepted 24 June 2009
Available online 28 June 2009

Keywords:
Molecular tweezers
Density functional theory
Dispersion forces
Spectroscopy

ABSTRACT

Molecular tweezers attracted attention because of their potential to selectively bind important chemicals, which can be utilized in medicine or in pollution treatment. In this study, the aromatic binding properties of a recently synthesized tweezer based on the Tröger's base and its complex with nitrobenzene are investigated ab initio, using the DFT and MP2 computations. The predicted geometries and energies of the complex with nitrobenzene are well comparable with the experimental data. The B3LYP and BPW91 functionals did not provide a stable binding, in contrast to the observation. Only addition of the empirical Grimme correction for the van der Waals forces, not present in conventional DFT, yielded results consistent with the experiment, MP2 computations, and similar benchmark models. The correction also caused minor improvements of the Raman and infrared spectra, but not in the entire region of vibrational frequencies. The results suggest that the role of the electrostatic interaction in the investigated complex is minor and the interaction stabilization is driven by the contact area between the polarizable aromatic systems. The vdW-DFT method thus provides an efficient tool for the rational synthesis of the complexes.

1. Introduction

The fascinating possibility to carry the functional drug to the target cell protected by a neutral compound has attracted attention of many organist chemists [1]. Using the carriers based on the Tröger's base appears especially convenient, as the relatively reactive polar site of the molecule can easily be modified in the organism and the tweezer arms can release the drug [2,3]. In order to achieve this goal, various derivatives have been proposed in the past, some of them exhibiting strong binding with model compounds [2].

The rational synthesis of the tweezers and search for new complexation agents can significantly be enhanced by the means of computational chemistry. For example, tweezers containing porphyrin moieties and metal ions were studied with the aid of the semiempirical AM1 and density functional theory (DFT) methods [4]. A significant attention was paid to the exploration of the dispersion van der Waals interactions that largely contribute to the stability of complexes with extended contact areas between the tweezer and carried compounds [5,6]. Indeed, molecular dynamics simulations confirmed the energetic convenience of the stacking for large aromatic systems [5]. In heteroaromatic molecules the electrostatic forces have an additional impact on the stability [6]. The linear scaling methods made it possible to compute NMR properties and large hydrated tweezer complexes [7].

However, the accuracy of the theoretical predictions is limited. Discrepancies between results obtained at various levels were reported for model clips, tweezers, and similar compounds [8]. Even for the modern density functional methods the proper account for the dispersion interaction is notoriously difficult, due to the locality of the available functionals [9]. This could be recently partially fixed by development of new functionals [10] or addition of an empirical correction the existing ones [11].

In this work we test the applicability of the density functional theory on the model Tröger's tweezer that was synthesized recently. Performance of the standard BPW91 (BPW) and B3LYP (B3L) functionals enhanced by the empirical Grimme dispersion correction is tested on model systems and compared to previous benchmark computation. The binding energies and complex geometries are compared to the experimental data. For the first time, the dispersion correction was applied to simulate the tweezer vibrational properties, but it did not bring a convincing improvement of the infrared and Raman spectra. Nevertheless, the dispersion-corrected DFT (DFT-D) did reliably predict other complex properties and thus can be used as a complementary tool for rational tweezer synthesis.

* Corresponding author.
E-mail addresses: vparchansky@gmail.com (V. Parchaňský), bour@uochb.cas.cz (P. Bouř).

0022-2860/$ - see front matter © 2009 Elsevier B.V. All rights reserved.
doi:10.1016/j.molstruc.2009.06.030

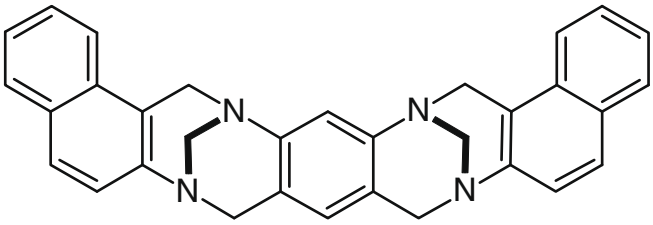

Fig. 1. The tweezer molecule in the syn-conformation.

2. Method

2.1. Experimental

The synthesis of the tweezer (T) compound (Fig. 1) was described in Ref. [12]. A titration of the tweezer with nitrobenzene (NB) in the $CHCl_3$ solution was monitored by the fluorescence spectroscopy. The association constant of the complex formation, T + NB → TNB, was determined from the florescence curve as $K = \frac{[TNB]}{[T][NB]} = (1200 \pm 400)$, which corresponds to a reaction free energy (ΔG) of about 4.1 kcal/mol at 298 K [3]. From a chloroform solution the tweezer and also its nitrobenzene complex were crystallized, and the geometry resolved by X-ray crystallography. The Raman spectrum of the compound was acquired in the solid state and in $CHCl_3$ solution. Further details of the fluorescence, X-ray and Raman experiments will be published elsewhere [3].

2.2. Calculations

The Gaussian [13] and Turbomole [14] programs were used for the quantum mechanical calculations of equilibrium geometries, energies, and spectroscopic molecular properties. Test computations on model complexes [15] were conducted at the MP2 and CCSD(T) levels to calibrate the DFT methodology. The DFT calculations were performed with the standard BPW91 [16] and B3LYP [17] functionals, as well as with those containing the dispersion correction as specified below. Standard Turbomole (SVP) and Pople-type Gaussian (6-31G, 6-31G**, 6-31++G**, 6-311++G**) basis sets were used, applying the density fitting acceleration [18] during the minimization for the larger set. The acceleration was switched off for a final calculation of the energy. The SVP results are not shown as they were very close to those obtained with the 6-31G** basis. The resolution of identity algorithm (RI) was used for MP2. Harmonic infrared absorption and Raman spectra were obtained from calculated frequencies and intensities using Lorentzian bands with an arbitrary bandwidth (full width at half height) of 5 cm^{-1}.

The Grimme dispersion energy correction [19] is

$$E = -s_6 \sum_i \sum_{j>i} \frac{c_{ij}}{r_{ij}^6} f(r_{ij}) \tag{1}$$

where r_{ij} is the distance between atoms i and j, $f(r_{ij}) = (1+ep)^{-1}$ is the damping function with $ep = \exp(-d(r_{ij}/R_r - 1))$, s_6 is a global scaling factor, $d = 20$, R_r is a sum of atomic van der Waals (vdW) radii, and c_{ij} are the dispersion coefficients. The parameter values can be found in the original reference [19]. They were obtained on the basis of SCS-MP2 benchmark computations on a large set of complexes including atoms and small molecules, as well as molecular dimers [20]. Later, these parameters were only slightly modified for a computational convenience [19]. From (1), we get the gradient and second-energy derivatives,

$$\frac{\partial E}{\partial r_{i\alpha}} = s_6 \sum_{j\neq i} \frac{c_{ij}}{r_{ij}^7} \left[\frac{6f(r_{ij})}{r_{ij}} - \frac{\partial f(r_{ij})}{\partial r_{ij}} \right] r_{ij\alpha}, \tag{2}$$

$$\frac{\partial^2 E}{\partial r_{i\alpha}\partial r_{i\beta}} = -s_6 \sum_{j\neq i} \frac{c_{ij}}{r_{ij}^8} \left[\left(\frac{48f(r_{ij})}{r_{ij}^2} - \frac{13}{r_{ij}} \frac{\partial f(r_{ij})}{\partial r_{ij}} + \frac{\partial^2 f(r_{ij})}{\partial r_{ij}^2} \right) r_{ij\alpha} r_{ij\beta} - \left(\frac{6f(r_{ij})}{r_{ij}^2} - \frac{\partial f(r_{ij})}{r_{ij}\partial r_{ij}} \right) r_{ij}^2 \delta_{\alpha\beta} \right], \tag{3a}$$

$$\left.\frac{\partial^2 E}{\partial r_{i\alpha}\partial r_{j\beta}}\right|_{j\neq i} = s_6 \frac{c_{ij}}{r_{ij}^8} \left[\left(\frac{48f(r_{ij})}{r_{ij}^2} - \frac{13}{r_{ij}} \frac{\partial f(r_{ij})}{\partial r_{ij}} + \frac{\partial^2 f(r_{ij})}{\partial r_{ij}^2} \right) r_{ij\alpha} r_{ij\beta} - \left(\frac{6f(r_{ij})}{r_{ij}^2} - \frac{\partial f(r_{ij})}{r_{ij}\partial r_{ij}} \right) r_{ij}^2 \delta_{\alpha\beta} \right], \tag{3b}$$

where $\frac{\partial f(r_{ij})}{\partial r_{ij}} = \frac{epd}{R_r} f(r_{ij})^2$ and $\frac{\partial^2 f(r_{ij})}{\partial r_{ij}^2} = [2epf(r_{ij}) - 1]\frac{epd^2}{R_r^2} f(r_{ij})^2$. These formulas were implemented within our version of the Gaussian program.

3. Results

3.1. Method validation

Currently, computations of sizable systems are often restricted to the density functional methods. However, as pointed out in many previous works [9,11,19], contemporary DFT functionals do not reproduce the long-range dispersion vdW interaction in full. As this can be most easily corrected by an empirical correction, such as that one described above, we test its performance on model systems relevant to the tweezer complex, three complexes of

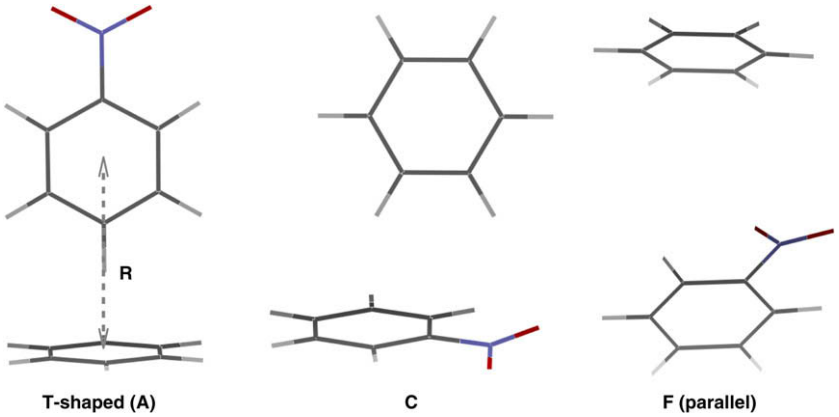

Fig. 2. Structures of the benzene–nitrobenzene complexes used for the calibration calculations. Geometries of **C** and **F** were fully optimized at the vdW-B3LYP/6-31G** level.

Table 1
Binding energies (kcal/mol) of three model benzene–nitrobenzene complexes (Fig. 2). The values calculated by the vdW-corrected DFT/6-31G** methods are compared to the benchmark wavefunction computations extrapolated to infinite basis.

ΔE	vdW-BPW91	vdW-B3LYP	MP2 [15]	CCSD(T) [15]
A	−3.54	−4.74	−3.91	−2.95
C	−2.06	−4.81	−3.10	−1.99
F	−4.24	−6.69	−7.21	−4.48

benzene and nitrobenzene (Fig. 2, using the original [15] names **A**, **C** and **F**) against more reliable wavefunction calculations. The calculated relative binding energies are listed in Table 1. As can be see, the DFT energies including the Grimme correction (vdW-DFT) faithfully copy the MP2 and CCSD(T) results obtained previously [15]. The B3LYP energies are somewhat higher than those calculated by the BPW91 method. The BPW91 values are closer to the presumably most accurate CCSD(T) values than for B3LYP.

The vdW-DFT method also provides qualitatively correct distance dependence of the energy, as documented in Fig. 3 for the T-shaped **A** complex. As shown in the left hand part of the figure, for a given basis set the DFT curve is reasonably close to the CCSD(T) and MP2 results. The CCSD(T) dependence indicates that the MP2 interaction energies might be somewhat overestimated, similarly as in Table 1. Unfortunately, only the smaller 6-31G basis could be used for the coupled cluster calculation due to the computer limits. Nevertheless, the vdW-DFT methods clearly gives at least qualitatively correct dependence of the intermolecular energy on the distance and reasonable estimation of the interaction energy, if compared with the wavefunction methods. Without the correction, no comparable minimum could be obtained, even in a larger basis set (cf. right-hand part of Fig. 3). Additionally, the vdW-DFT curves seem to be less dependent on the basis set size than those obtained by the MP2 method (cf. the 6-31G and 6-311++G** basis sets).

3.2. The tweezer–nitrobenzene complex geometry

Neither the BPW91 nor the B3LYP functional with any basis we tried (6-31G, 6-31G** and 6-311++G**) gave a stable binding of the nitrobenzene ligand to the tweezer. Typically, the ligand was expelled out of the tweezer pocket. However, the corrected functionals (vdW-BPW91 and vdW-B3LYP) provided a stable geometry that is very close to that found by X-ray (Fig. 4). Similar equilibrium structure was obtained at the MP2/6-31G** level. The X-ray geometry possesses a planar (C_s) symmetry, and this was reproduced by all the computations. This also suggests a relatively tight packing and a binding restriction to small molecules as ligands, such as

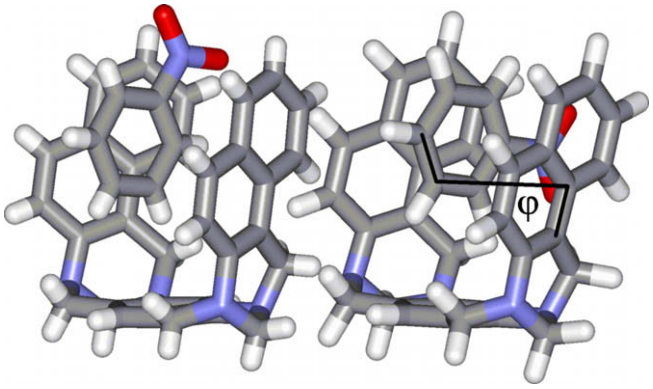

Fig. 4. Comparison of the (left) X-ray and (right) vdW-BPW91/6-31G** optimized geometry of the tweezer–NB complex. Definition of the twist angle is given on the right hand side.

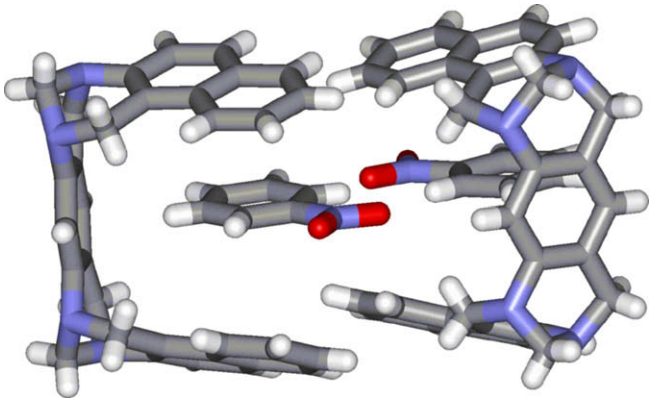

Fig. 5. The X-ray structure containing two tweezer–nitrobenzene units.

the flat phenyl ring in the nitrobenzene that fills the space between the tweezer's arms.

The nitrobenzene group in the calculated equilibrium geometries, however, is somewhat differently oriented than in the crystal with respect to the φ-angle (Fig. 4). We attribute this to a shallow potential of the rotation and forces acting in the solid state. Indeed, in the crystal, the nitrobenzene molecules form approximately planar chains (Fig. 5) with some kind of hydrogen bond between the aromatic hydrogen and NO_2 oxygen atoms. The potential calculated at the DFT level is shown in Fig. 6. It exhibits a global minimum ($\varphi \sim 150°$). To adopt the geometry in the crystal ($\varphi \sim 90°$)

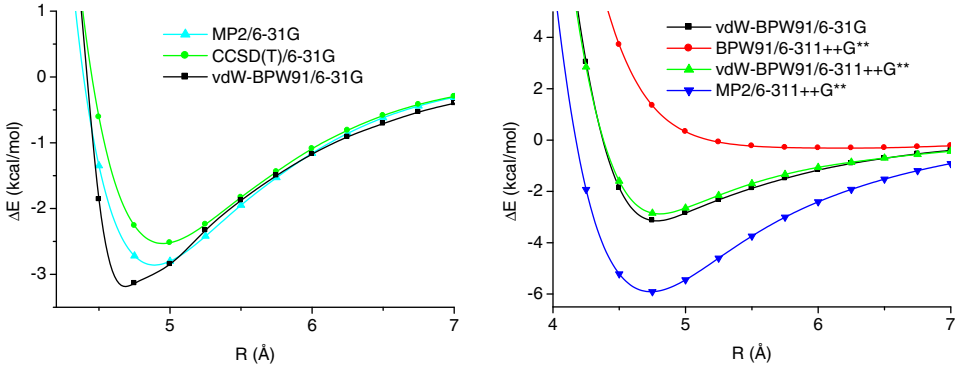

Fig. 3. Nitrobenzene and benzene, comparison of the interaction energy as a function of the distance, for the **A** complex (Fig. 2). Left: MP2, CCSD(T) and vdW-DFT calculations in the 6-31G basis, right: the MP2/6-311++G** calculation and various BPW91 models.

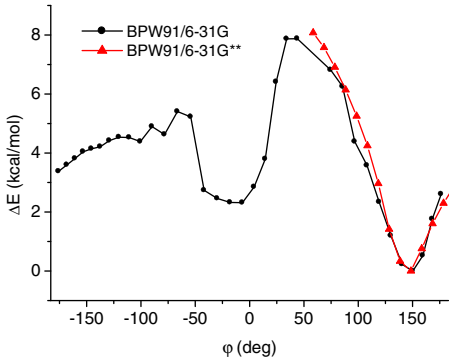

Fig. 6. Calculated dependence of the relative energy of the tweezer–nitrobenzene complex on the twist angle defined in Fig. 4. In the X-ray geometry, $\varphi \sim 90°$.

the energy of the monomer complex would need to increase to about 4 kcal/mol.

The calculated potential curve roughly corresponds to the electrostatic potential of the nitrobenzene and tweezer (Fig. 7), in that the negatively-charged NO_2 terminus points out from the negative inside of the tweeze pocket (red regions). But as indicated by the computation of the benchmark complexes, the stabilization energy seems to be governed rather by the dispersion interactions and sterical effects than by electrostatic attractions and repulsions. The finer tuning of the complex geometry by the electrostatically functioning groups, however, appears interesting for potential application.

3.3. The tweezer complex binding energies

In spite of the dominance of the van der Waals terms, notable differences exist between the relative complex energies calculated at various approximation levels. These are in Table 2 evaluated not only for the complex with nitrobenzene, but also for common solvent molecules, as in real complexes competition with the solvent must be considered. The DFT computation without the vdW correction (second column in Table 2) provides quite unrealistic binding energies; also the geometries (not shown) are quite different than, for example, those obtained by the more reliable MP2 computation.

With the correction, the GGA BPW91 functional gives stabilization energies by up to ~30% smaller than the MP2 and B3LYP methods. The zero point vibrational energy correction is relatively small for nitrobenzene, but may become important for a weakly bonded ligand, such as CH_4. The vdW-BPW results obtained with the 6-31G** and 6-311++G** (last column) basis sets are quite similar. For the BPW91 functional the vacuum energies agree well with those obtained with the PCM solvent ($CHCl_3$) correction, which is in accord with the dominance of the van der Waals interactions. The energies of the complex with the water molecule seems to be most affected by the approximation level, probably because of a complicated interplay between the vdW, electrostatic, and polarization effects.

In agreement with the experimental data, we can see (Table 2) that the nitrobenzene–tweezer complex is the strongest (with stabilization energy of 20–28 kcal/mol). Perhaps surprisingly, sole benzene provides only about half of the stabilization energy, and water is bond relatively strongly due to the polar hydrogen binding to the tweezer nitrogen atoms. In potential applications one can speculate that the complex with the ligand can slowly be released by the solvent without further agents. Most probably, however, a more specific binding (with higher stabilization energy) would be needed for usage of the tweezer as a reliable ligand carrier.

In order to understand more of the tweezer-ligand interaction energetic, we calculated stabilization energies of complexes between nitrobenzene and the central and terminal part of the tweezer (Table 3). As can be seen in the Table, the energy is approximately additive, which is consistent with the prevalent vdW interaction scheme.

Table 2
Relative energies (in kcal/mol) of tweezer complexes with various ligands calculated at seven approximation levels.

Ligand	6-31G**						6–311++G**
	BPW	vdW-BPW	vdW-BPW[a]	vdW-BPW[b]	RI-MP2	vdW-B3L	vdW-BPW
Nitrobenzene	0.6	20.0	17.0	16.0	27.3	27.6	18.8
$CHCl_3$	−0.6	6.6	6.3	7.1	8.7	11.3	7.6
C_6H_6	0.1	9.0	7.2	8.3	13.0	14.3	8.5
H_2O	5.3	11.7	9.3	9.3	10.2	14.7	7.7
CH_4	0.1	4.7	2.5	4.8	4.1	8.7	4.9
CCl_4	0.3	5.8	5.5	5.7	8.9	11.1	7.2

[a] ZPE correction included.
[b] CPCM solvent model ($CHCl_3$).

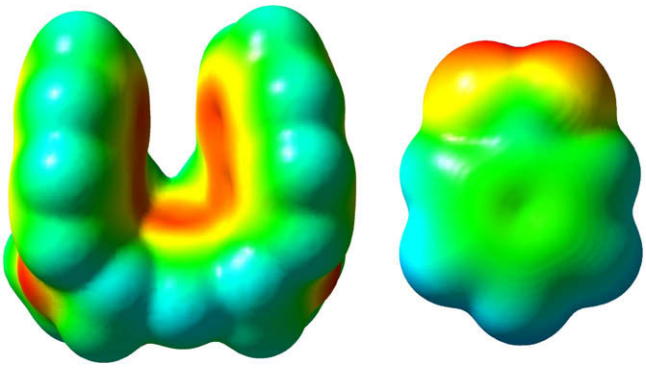

Fig. 7. Electrostatic potential on the vdW surface of the tweezer (left) and nitrobezene (right). Positive and negative regions have blue and red color, respectively. (For interpretation of the references to color in this figure legend, the reader is referred to the web version of this article.)

Table 3
Calculated creation energies (vdW- BPW91/6-31G**) of model complexes mimicking part of the tweezer molecule.

System	ΔE (kcal/mol)
1 NB + 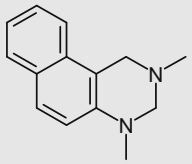	8.8
2 NB + 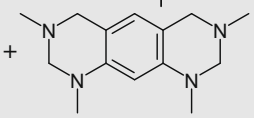	8.1
sum 1 + 1 + 2	25.0
3 NB + 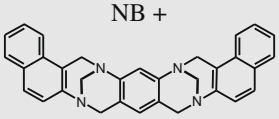	20.0

3.4. Tweezer vibrational spectra

Raman and IR spectroscopy is often used to characterize the purity and interactions of the compounds involved in the complexes. Although we did not succeed so far in measurement of the complex spectra, good agreement was achieved between the simulated and experimental spectra of the sole tweezer. The experimental IR spectra in $CHCl_3$ solution and KBr pellet are compared to the calculation (B3LYP/6-31++G**/PCM($CHCl_3$)) in Fig. 8. The BPW91 functional and B3LYP with a small 6-31G** basis provided similar and slightly inferior spectra (not shown). The frequencies of the strongest bands are summarized in Table 4 and completed by the Raman scattering data from the solid state and $CHCl_3$ solution (cf. also Fig. 9). Both for Raman and IR, the solid and solution spectra are very similar; hence only the solution is reported in the Table.

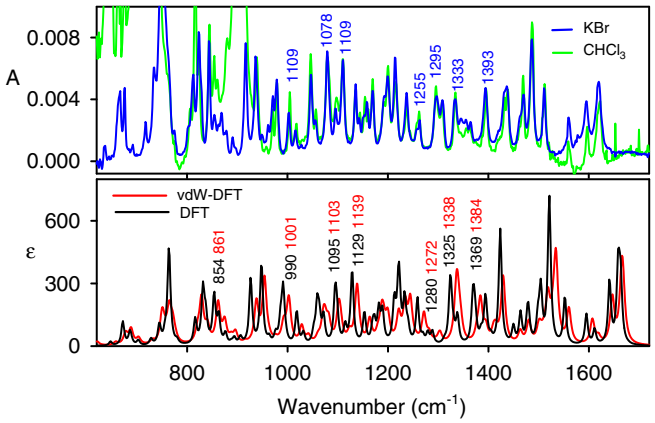

Fig. 8. Experimental IR spectra of the tweezer in chloroform solution and KBr pellet (top) and the spectra simulated (B3LYP/6-31++G**/CPCM) with and without the vdW correction (bottom).

Table 4
Calculated DFT-B3LYP6-31++G**/CPCM($CHCl_3$) and experimental tweezer vibrational frequencies (cm^{-1}).

Calc		Exp/$CHCl_3$		Calc		Exp/$CHCl_3$	
DFT	vdW-DFT	IR	Raman	DFT	vdW-DFT	IR	Raman
1663	1666	1619	1623	1031	1041	1016	1018
1641	1647	1597	1599	1018	1028	1005	
1611	1608	1577	1578	991	1003	979	977
1595	1619	1560	1563	986	992	971	
1552	1560	1512		948	954	939	
1521	1534	1486		888	888		890
1504	1518	1469	1511	863	875		855
1481			1470	837	840		825
1479			1463	816	821		810
1478	1500	1439		756	771		756
1464	1480	1431	1433	744	754		735
1450	1463	1419		692	702		676
1423	1429	1396	1396	672	688		664
1405	1415		1375	607	621		600
1394	1410	1361		576	584		569
1385	1394		1356	564			549
1372	1384	1334		539	547		531
1369	1344	1334	1308	531			524
1338	1341	1308	1308	518	517		513
1324	1337	1296	1297	489	488		483
1279	1300		1259	451	454		447
1259	1272	1237	1238	429	429		424
1240	1244	1215		422	420		414
1223	1234	1200		413	411		406
1212	1121	1193		377	385		384
1189	1199	1170		365	360		363
1182	1188	1160		330	335		331
1173	?	1155					285
1169	1181	1143	1154	280	285		276
1153	1164	1136	1143	275	276		260
1128	1139	1110					243
1115	1123	1096	1096	228			233
1095	1101	1080		203	201		208
1072	1082	1056		183	191		190
1059	1071	1047		174	166		183
1052	1061		1031				
δ				17	16		0

δ – mean deviation between the calculation and the experiment.

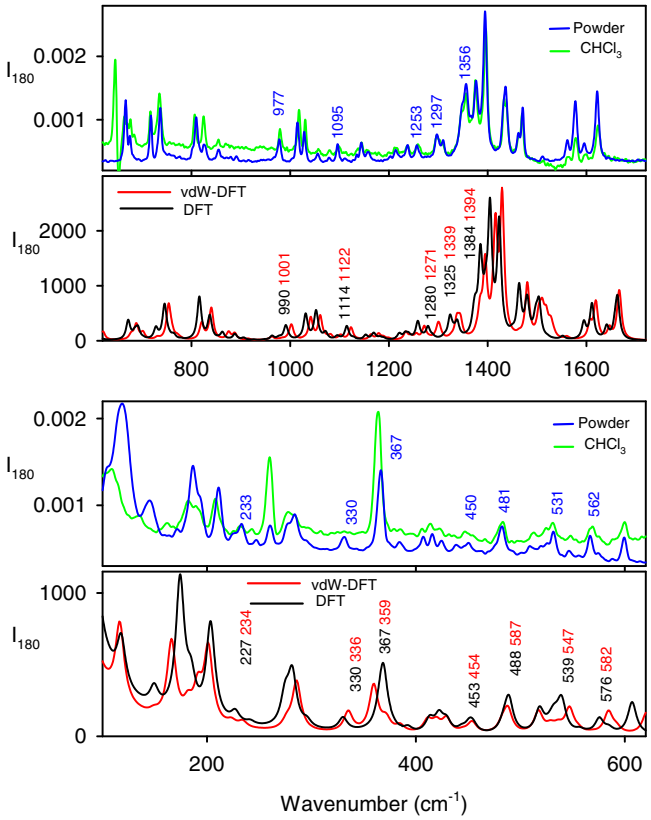

Fig. 9. Experimental Raman spectra of the tweezer in chloroform solution and powder (top) and the spectra simulated (B3LYP/6-31++G**/CPCM) with and without the vdW correction (bottom).

As can be seen in Figs. 8 (IR) and 9 (Raman), most of the observable transitions could be assigned and related to the simulated bands. The calculated frequencies within the region dominated by C=C aromatic stretching (~1360–1625 cm^{-1}) are slightly higher than experimental ones. The agreement of the intensity pattern of the hydrogen bending region (~1130–1360 cm^{-1}) is rather poor, although most of the bands could be assigned as well. The vdW correction does not significantly improve an overall agreement with the experimental frequencies (cf. the mean deviations of 17 and 16 cm^{-1} for the uncorrected and corrected frequencies in Table 4), but it brings occasional positive effects for the hydrogen bending bands. This is understandable as the interactions of the hydrogen atoms that are on the molecular surface is in a large part mediated by the vdW forces.

4. Conclusions

We have analyzed the nitrobenzene–tweezer complex in terms of the stabilization energy and geometry. On the model systems, the vdW(dispersion)-corrected DFT provided results comparable with higher-level wavefunction calculations. For the tweezer, it resulted into geometry, stabilization energy, and vibrational spectra well comparable with the experiment. The dispersion energy that is roughly proportional to the contact area between the aromatic

residues was determined as the main stabilization factor. The electrostatic forces played a minor role for the aromatic complex, but could be dominant for water molecules and similar polar ligands. The vdW interactions significantly contribute to the shape of simulated spectra, but there role is masked by other inaccuracies of the DFT computational model. Nevertheless, the simulations seem to be a reliable and important tool for a rational design of similar drug-carrying compounds in the future.

Acknowledgment

This work was supported by the Czech Grant Agency (Grants 202/07/0732 and 203/08/1445), the Grant Agency of the Academy of Sciences (A4005507020, M200550902), and Ministry of Education of the Czech Republic (MSM 6046137307).

References

[1] J.L. Atwood, J.W. Steed, Supramolecular Chemistry, Wiley, Weinheim, 2000.
[2] M. Valík, P. Matějka, E. Herdtweck, V. Král, B. Dolenský, Collect. Czech. Chem. Commun. 71 (2006) 1278.
[3] M. Havlík, V. Parchaňský, P. Bouř, V. Král, B. Dolenský, Collect. Czech. Chem. Commun. 7–8 (2009), in press.
[4] D. Margetic, R.N. Warrener, D.N. Butler, D. Officer, Theor. Chem. Acc. 117 (2007) 239.
[5] W.L. Jorgensen, D.L. Severance, J. Am. Chem. Soc. 112 (1990) 4768.
[6] Y. Chang, Y. Chen, C. Chen, Y. Wen, J. Lin, H. Chen, M. Kuo, I. Chao, J. Org. Chem. 73 (2008) 4608–4614.
[7] C. Ochsenfeld, J. Kussmann, F. Koziol, Angew. Chem. Int. Ed. Engl. 43 (2004) 4485.
[8] G.F. Klarner, J. Panitzky, D. Preda, L.T. Scott, J. Mol. Model. 6 (2000) 318.
[9] V. Špirko, O. Engkvist, P. Soldán, H.L. Selzle, E.W. Schlang, P. Hobza, J. Chem. Phys. 111 (1999) 572;
J. Šponer, P. Hobza, Collect. Czech. Chem. Commun. 68 (2003) 2231;
J. Černý, P. Hobza, Phys. Chem. Chem. Phys. 7 (2005) 1624;
P. Hobza, J. Sponer, Chem. Rev. 99 (1999) 3247.
[10] J.W. Song, S. Tokura, T. Sato, M.A. Watson, K. Hirao, J. Chem. Phys. 127 (2007) 154109.
[11] T. Schwabe, S. Grimme, Phys. Chem. Chem. Phys. 9 (2007) 3397.
[12] M. Havlík, V. Král, B. Dolenský, Org. Lett. 8 (2006) 4867.
[13] M.J. Frisch, G.W. Trucks, H.B. Schlegel, G.E. Scuseria, M.A. Robb, J.R. Cheeseman, J. Montgomery, J.A., T. Vreven, K.N. Kudin, J.C. Burant, J.M. Millam, S.S. Iyengar, J. Tomasi, V. Barone, B. Mennucci, M. Cossi, G. Scalmani, N. Rega, G.A. Petersson, H. Nakatsuji, M. Hada, M. Ehara, K. Toyota, R. Fukuda, J. Hasegawa, M. Ishida, T. Nakajima, Y. Honda, O. Kitao, H. Nakai, M. Klene, X. Li, J.E. Knox, H.P. Hratchian, J.B. Cross, V. Bakken, C. Adamo, J. Jaramillo, R. Gomperts, R.E. Stratmann, O. Yazyev, A.J. Austin, R. Cammi, C. Pomelli, J.W. Ochterski, P.Y. Ayala, K. Morokuma, G.A. Voth, P. Salvador, J.J. Dannenberg, V.G. Zakrzewski, S. Dapprich, A.D. Daniels, M.C. Strain, O. Farkas, D.K. Malick, A.D. Rabuck, K. Raghavachari, J.B. Foresman, J.V. Ortiz, Q. Cui, A.G. Baboul, S. Clifford, J. Cioslowski, B.B. Stefanov, G. Liu, A. Liashenko, P. Piskorz, I. Komaromi, R.L. Martin, D.J. Fox, T. Keith, M.A. Al-Laham, C.Y. Peng, A. Nanayakkara, M. Challacombe, P.M.W. Gill, B. Johnson, W. Chen, M.W. Wong, C. Gonzalez, J.A. Pople, Gaussian 03, Revision C.02 (Gaussian, Inc., Wallingford CT, 2004).
[14] R. Ahlrichs, M. Bar, H.-P. Baron, R. Bauernschmitt, S. Bocker, M. Ehrig, K. Eichkorn, S. Elliot, F. Furche, F. Haase, M. Haser, H. Horn, C. Huber, U. Huniar, M. Kattannek, C. Kolmel, M. Koolwitz, K. May, C. Ochsenfeld, H. Ohm, A. Schafer, U. Schneider, O. Treutler, M. von Arnim, F. Weigend, P. Weis, and H. Weiss, Turbomole, version 5 (Quantum Chemistry Group, University of Karlsruhe., Karlsruhe, 1998).
[15] S. Tsuzuki, K. Honda, T. Uchimaru, M. Mikami, J. Chem. Phys. 125 (2006) 124304.
[16] A.D. Becke, in: D.R. Yarkony (Ed.), Modern Electronic Structure Theory, vol. 2, World Scientific, Singapore, 1995, p. 1022.
[17] A.D. Becke, J. Chem. Phys. 98 (1993) 5648.
[18] N. Godbout, D.R. Salahub, J. Andzelm, E. Wimmer, Can. J. Chem. 70 (1992) 560.
[19] S. Grimme, J. Comp. Chem. 27 (2006) 1787–1799.
[20] S. Grimme, J. Comp. Chem. 25 (2004) 1463–1473.